Northern blot analysis. A cDNA probe spanning BRI nucleotides 268 to 969 (named p701) was hybridized to northern blots (Clontech) containing 2 μg per lane of human poly-A^+ mRNA isolated from different tissues and various regions of the human brain. Filters were prehybridized at 42 °C for 3 h in 5 × SSC, 5 × Denhards, 20 mM NaH_2PO_4, 0.2% SDS, 20% formamide and 250 μg ml^{-1} salmon sperm DNA. Hybridization was performed for 16 h at 42 °C in the same solution containing the ^{32}P-labelled p701 probe at 1 × 10^6 c.p.m. per ml. Membranes were washed at 42 °C in 2 × SSPE containing 0.1% SDS. Blots were rehybridized in ExpressHyb solution (Clontech) at 68 °C for 1 h using the ^{32}P-labelled β-actin probe.

Southern blot analysis. Ten micrograms of genomic DNA for Southern blot analysis (Clontech) was digested with *Bam*HI, size-fractionated on 1% agarose gel, blotted onto a nitrocellulose filter and hybridized to ^{32}P-labelled p701 probe at 42 °C. After post-hybridizational washes at 65 °C in 2 × SSC, 0.1% SDS, the blots were exposed to X-ray film at −80 °C.

Restriction analysis. Amplification of genomic DNA samples isolated from peripheral blood leukocytes of living family members and autopsy tissue was done using oligonucleotide primer pairs F (5′-CGTGAAGCCAGCAATT GTTTCGCA-3′) and R (5′-AGCCCTGTTTGCTACTTACATG-3′) (the product was 191 bp) by PCR using 250 μmol dNTPs, 2.5 mM $MgCl_2$, 50 pmol oligonucleotides, in 100 μl, and cycled for 30 cycles of 94 °C for 30 s, 50 °C for 30 s and 72 °C for 30 s. PCR products were cloned and sequenced by automated cycle sequencing. Analysis of the amplified PCR products was done with the restriction enzyme *Xba*I (Gibco, BRL) according to the manufacturer's instructions, and the resulting products were resolved by non-denaturing 5% polyacrylamide gel electrophoresis.

Immunohistochemistry. The 4K purified ABri amyloid as well as a synthetic peptide CTVKKNIIEEN, which is homologous to the ten C-terminal residues of the ABri molecule and which contains an extra N-terminal cysteine for coupling to keyhole limpet haemocyanin, were used to induce a polyclonal antibody response in rabbits. After an initial stimulation with 200 μg of antigen emulsified in monophospholipid A-synthetic trehalose dicorynomycolate (RIBI; Immunochem Research) adjuvant, animals were boosted with 50 μg of antigen every three weeks for twelve weeks. Specific antibodies were tested by enzyme-linked immunosorbent assay (ELISA) and dot-blot analysis against a synthetic peptide that was homologous to the full-length ABri sequence. Immunoglobulin-γ (IgG) fractions were purified from the rabbit serum by means of specific binding to protein G (Gammabind G, Pharmacia). Immunoadsorption of both antibodies was done with full-length ABri peptide (100 μg of peptide per 50 μl of antibody) for 1 h at 37 °C and 16 h at 4 °C, followed by centrifugation at 14,000*g* for 5 min. Temporal adjacent sections of case V41 (ref. 1) were immunostained with both antibodies followed by biotinylated anti-rabbit IgG and streptavidine–horseradish peroxidase (HRP). Colour was developed with diaminobenzidine tetrahydrochloride (DAB) and hydrogen peroxide.

Received 15 February; accepted 4 May 1996.

1. Plant, G. T., Révész, T., Barnard, R. O., Harding, A. E. & Gautier-Smith, P. C. Familial cerebral amyloid angiopathy with nonneuritic plaque formation. *Brain* **113,** 721–747 (1990).
2. Worster-Drought, C., Hill, T. R. & McMenemey, W. H. Familial presenile dementia with spastic paralysis. *J. Neurol. Psychopathol.* **14,** 27–34 (1933).
3. Worster-Drought, C., Greenfield, J. G. & McMenemey, W. H. A form of familial presenile dementia with spastic paralysis (including the pathological examination of a case). *Brain* **63,** 237–254 (1940).
4. Worster-Drought, C., Greenfield, J. G. & McMenemey, W. H. A form of presenile dementia with spastic paralysis. *Brain* **67,** 38–43 (1944).
5. Corsellis, J. & Brierley, J. B. An unusual type of presenile dementia: (atypical Alzheimer's disease with amyloid vascular change). *Brain* **77,** 571–587 (1954).
6. Aikawa, H., Suzuki, K., Iwasaki, Y. & Iizuka, R. Atypical Alzheimer's disease with spastic paresis and ataxia. *Ann. Neurol.* **17,** 297–300 (1985).
7. Masters, C., Gajdusek, C. & Gibbs, C. J. The familial occurrence of Creutzfeldt-Jakob disease and Alzheimer's disease. *Brain* **104,** 535–558 (1981).
8. Keohane, C., Peatfield, R. & Duchen, L. W. Subacute spongiform encephalopathy (Creutzfeldt-Jakob disease) with amyloid angiopathy. *J. Neurol. Neurosurg. Psych.* **48,** 1175–1178 (1985).
9. Courten-Myers, G. & Mandybur, T. I. Atypical Gerstmann-Straüssler syndrome or familial spinocerebellar ataxia and Alzheimer's disease? *Neurology* **37,** 269–275 (1987).
10. Pearlman, R. L., Towfight, J., Pezeshkpour, G. H., Tenser, R. B. & Turel, A. P. Clinical significance of types of cerebellar amyloid plaques in human spongiform encephalopathies. *Neurology* **38,** 1249–1254 (1988).
11. Vinters, H. Cerebral amyloid angiopathy: a critical review. *Stroke* **18,** 311–324 (1987).
12. Ghiso, J., Plant, G. T., Révész, T., Wisniewski, T. & Frangione, B. Familial cerebral amyloid angiopathy (British type) with nonneuritic amyloid plaque formation may be due to a novel amyloid protein. *J. Neurol. Sci.* **129,** 74–75 (1995).
13. Baumann, M. H., Wisniewski, T., Levy, E., Plant, G. T. & Ghiso, J. C-terminal fragments of α- and β-tubulin form amyloid fibrils *in vitro* and associate with amyloid deposits of familial amyloid angiopathy, British type. *Biochem. Biophys. Res. Commun.* **219,** 238–242 (1996).
14. Révész, T. *et al.* Cytoskeletal pathology in familial amyloid angiopathy (British type) with non-neuritic plaque formation. *Acta Neuropath.* **97,** 170–176 (1999).
15. Altschul, S. F. *et al.* Gapped BLAST and PSI-BLAST: a new generation of protein database search programs. *Nucleic Acids Res.* **25,** 3389–3402 (1997).
16. Kozak, M. An analysis of 5′-noncoding sequences from 699 vertebrate messenger RNA. *Nucleic Acids Res.* **15,** 8125–8148 (1987).
17. Kyte, J. & Doolittle, R. F. A simple method for displaying the hydropathic character of a protein. *J. Mol. Biol.* **157,** 105–132 (1982).
18. Sonnhammer, E. L., von Heijne, G. & Krogh, A. A hidden Markov model for predicting transmembrane helices in protein sequences. *I.S.M.B.*, **6,** 175–182 (1998).
19. Deleersnijder, W. *et al.* Isolation of markers for chondro-osteogenic differentiation using cDNA library subtraction. *J. Biol. Chem.* **271,** 19475–19482 (1996).
20. Ghiso, J., Wisniewski, T. & Frangione, B. Unifying features of systemic and cerebral amyloidosis. *Mol. Neurobiol.* **8,** 49–64 (1994).
21. Vidal, R. *et al.* Meningocerebrovascular amyloidosis associated with a novel transthyretin mis-sense mutation at codon 18 (TTRD18G). *Am. J. Pathol.* **148,** 361–366 (1996).
22. Crook, R. *et al.* A variant of Alzheimer's disease with spastic paraparesis and unusual plaques due to deletion of exon 9 of presenilin 1. *Nature Med.* **4,** 452–455 (1998).
23. Ghetti, B. *et al.* Vascular variant of prion protein cerebral amyloidosis with tau-positive neurofibrillary tangles: the phenotype of the stop codon 145 mutation in PRNP. *Proc. Natl Acad. Sci. USA* **93,** 744–748 (1996).

Acknowledgements. This work was supported by the NIA LEAD award Alzheimer's disease and amyloid proteins (B.F.). J.G. is the recipient of the NIDA from AHA (NYC affiliate).

Correspondence and requests for materials should be addressed to J.G. (e-mail: ghisoj01@popmail.med.nyu.edu).

Human theta oscillations exhibit task dependence during virtual maze navigation

Michael J. Kahana*†, Robert Sekuler*†, Jeremy B. Caplan*, Matthew Kirschen* & Joseph R. Madsen*†‡

* *Volen Center for Complex Systems, Brandeis University, Waltham, Massachusetts 02454, USA*

† *Department of Neurosurgery, Children's Hospital, Boston, Massachusetts 02115, USA*

‡ *Department of Surgery, Harvard Medical School, Boston, Massachusetts 02115, USA*

Theta oscillations (electroencephalographic activity with a frequency of 4–8 Hz) have long been implicated in spatial navigation in rodents[1–3]; however, the role of theta oscillators in human spatial navigation has not been explored. Here we describe subdural recordings from epileptic patients learning to navigate computer-generated mazes. Visual inspection of the raw intracranial signal revealed striking episodes of high-amplitude slow-wave oscillations at a number of areas of the cortex, including temporal cortex. Spectral analysis showed that these oscillations were in the theta band. These episodes of theta activity, which typically last several cycles, are dependent on task characteristics. Theta oscillations occur more frequently in more complex mazes; they are also more frequent during recall trials than during learning trials.

Theta oscillations are seen when animals engage in a variety of spatial, motor and cognitive tasks[1–9]. For example, when rodents explore environments, theta oscillations are specifically related to the firing of hippocampal place cells that encode the animals' position[2,3]. Such findings have led researchers to assign a crucial functional role to the theta activity in physiologically based models of behaviour[10–12]. Although most studies of theta waves in rodents focus on the hippocampus and the role of the medial septum, they have also been seen in other brain regions, including the hypothalamus, entorhinal cortex, cingulate cortex and superior colliculus[13–15]. It is unclear whether cortical theta activity results from cortico-hippocampal interactions or the presence of multiple theta generators. There has been uncertainty over the existence (and possible functional role) of task-dependent theta activity in humans[16–18]. To help resolve this uncertainty we devised a spatial learning task for humans that resembles those tasks that elicit strong theta oscillations in rodents.

Although neuroimaging studies have examined brain activity during spatial navigation and wayfinding tasks[19–23], the techniques

used (positron emission tomography and functional magnetic resonance imaging) lack the temporal resolution needed to observe spectrally distinct brain activity such as theta oscillations. We have recorded intracranially from multiple cortical loci in humans who are exploring an unfamiliar, computer-simulated environment. Our results demonstrate both the existence and task dependence of theta oscillations during maze learning.

We tested three patients with medically intractable epilepsy who had arrays of subdural electrodes implanted for one to two weeks to localize the site or sites of seizure onset. The placement of these arrays was determined by the clinical team so as to best localize suspected epileptogenic foci and to identify functional regions to be avoided in surgery.

Unlike scalp electroencephalograms (EEG), intracranial EEG (iEEG) provides direct access to population activity in theoretically important cortical regions located on the brain's ventral surface. In addition, iEEG offers improved spatial resolution without attenuation of brain signals by the skull and scalp. iEEG also avoids muscle artefacts, including eye movements[24].

Subjects used a computer keyboard to navigate through visually rich, computer-rendered, three-dimensional mazes. Each virtual maze comprised a series of corridors, each leading to a T-junction (Fig. 1a). The subject's aim was to navigate as quickly and accurately as possible from a starting point to a goal position.

Subjects traversed each maze in two modes, denoted Study and Test. In Study mode, arrows placed at junctions directed subjects through the maze (Fig. 1b). In Test mode, the arrows were removed, forcing subjects to rely on a learned representation of the maze. Subjects navigated each maze four times in Study mode, and then navigated the same maze in Test mode until they could traverse the maze three times successively without errors.

Figure 2a shows a sample iEEG trace recorded from an electrode on the inferior frontal gyrus in subject 1 (Talairach[25] coordinates: L–R = −49, A–P = +21, I–S = −4 mm). This trace represents brain activity during a single maze traversal in Test mode. The complex waveform is interrupted by episodes of rhythmic slow-wave activity (Fig. 2a). These slow waves are in the theta range and appear during both Study and Test trials in all three subjects, and in many brain regions.

Our finding that theta activity is not continuous but occurs in distinct, well defined episodes can be seen in the frequency–time spectrogram (Fig. 2b) for each maze. *Z*-scores, thresholded at $z = 1$, are plotted for task power relative to the distribution of power across all maze trials (both long and short). The overall peak in the theta range can be seen consistently across both Study and Test trials (Fig. 2c).

To determine how theta episodes were related to specific attributes of our maze-learning task we compared power spectra obtained during long (12-junction) and short (6-junction) mazes. We had previously established that 12-junction mazes pose a serious challenge for any inexperienced subject, whereas 6-junction mazes are typically mastered by the first test trial (data not shown). Consistent with these normative findings, our three subjects took approximately 10 trials to learn long mazes, but only one or two learning trials to master short mazes. To test whether theta activity was sensitive to the increased cognitive demands of the long mazes we compared the probability of a theta episode occurring during performance of long versus short mazes. For each subject, at certain cortical loci, the percentage of maze trial time spent in theta episodes (P_θ) was greater for long mazes than for short mazes ($P < 0.01$ by a two-tailed Mann-Whitney *U*-test). In those electrodes showing significantly higher P_θ for long mazes as compared with short mazes, mean P_θ was 15% for long mazes and 10% for short mazes.

The median duration of theta episodes in long mazes was 720 ms (95th percentile = 1,630 ms) and in short mazes the median duration was 685 ms (95th percentile = 1,405 ms). These values were computed only across electrodes that showed a significant effect of maze complexity. We found no electrodes that recorded more theta

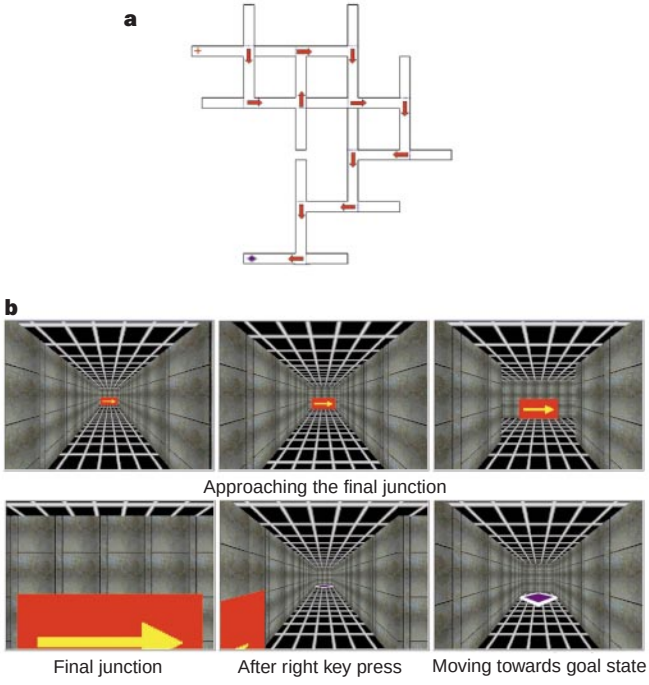

Figure 1 Navigation of computer-rendered multiple T-junction mazes. **a**, Blueprint of a sample 12-junction maze. Plus sign marks start position; diamond marks finish position. Arrows indicate the correct path. Dotted lines mark invisible barriers. **b**, Six sample views of the virtual environment, such as a subject would see when traversing a maze.

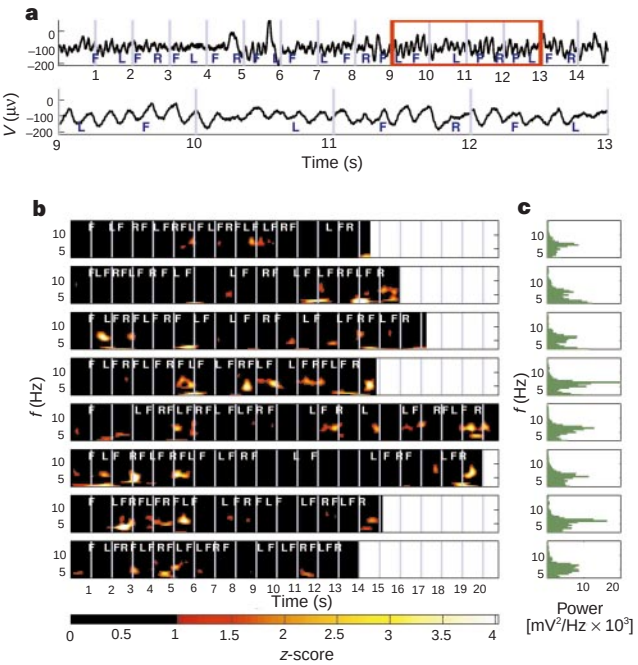

Figure 2 Theta oscillations revealed by intracranial EEG. **a**, Upper trace, sample iEEG trace from study trial 4, maze 15 recorded from an electrode on the inferior frontal gyrus in subject 1. Key presses are indicated by F (forward), R (right) and L (left). Lower trace, enlarged view of the boxed region, emphasizing the theta oscillation. **b**, Time-frequency spectrograms for all trials in maze 15 recorded from the same electrode as in **a**. The colour scale (bottom) reflects *z*-score relative to wavelet-window power across all maze trials. Rows 1–4, study trials; row 5, a test trial in which the subject made an error; rows 6–8, error-free test trials. **c**, Average power for each trial.

activity for short mazes than for long mazes. The locations of the 48 (out of 171) electrodes that exhibited this task complexity effect are shown in Fig. 3a–c. This difference in P_θ also showed up as a difference in the average power spectra for most of the significant electrodes, with the same direction of difference between long and short maze trials (Fig. 3d–g).

Research on learning has been advanced by the theoretical distinction between encoding and retrieval processes[26]. To investigate whether theta activity might have a different role in retrieval from its role in encoding we examined theta episodes separately in the first four Study trials and the final three Test trials across all mazes. In 45 electrodes, theta episodes occurred more frequently during Test trials than during Study trials ($P < 0.01$). No electrodes showed the reverse pattern.

As has been found in rodents, theta oscillations in our experiments with human subjects occur during spatial navigation. These oscillations are visually striking against a complex background signal. However, our recordings are from the cortical surface and not from the hippocampus itself. Further work is required before we can make precise statements about the link between our observation of human theta waves and the literature on hippocampal and cortical theta activity in rodents.

Because our observations came only from individuals with epilepsy, we cannot guarantee that non-epileptic brains would show theta oscillations identical to those reported here. To reduce the sensitivity of our analysis to epileptic artefacts, we focused not on the presence of theta activity *per se*, but on the task-related properties of theta episodes. Additionally our results are not artefacts of the intermittent sharp transients (70–200 ms) sometimes seen in epileptic brains. Indeed, our results are essentially unchanged when the criterion for a theta episode is decreased from 500 to 167 ms. Further, although in subjects 2 and 3 there is some overlap between the epileptogenic tissue and the electrodes showing task-related theta activity, in subject 1, whose raw signal showing theta oscillations is illustrated in Fig. 2, electrodes showing task-related theta were not near the clinically identified epileptogenic focus.

In summary, our spatial learning task not only reveals clear evidence of theta activity, but also shows that it occurs in distinct, task-dependent episodes. Because these theta episodes become more frequent in long mazes and during retrieval, it is likely that theta oscillations are important in human spatial cognition. □

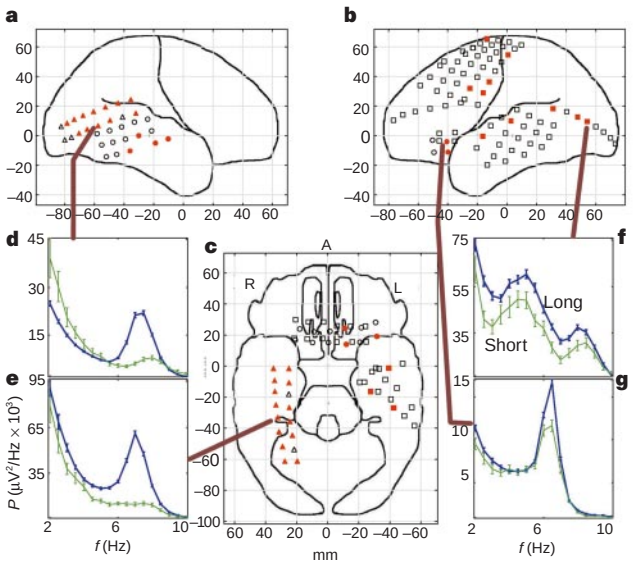

Figure 3 Electrode locations and task-dependent theta activity seen for all three subjects, shown on three diagrams of a standard brain. **a**, Right lateral view. **b**, Left lateral view. **c**, Inferior view. Circles, triangles and squares represent electrodes in subjects 1, 2 and 3, respectively. Electrodes filled in red recorded increased theta activity during long mazes relative to short mazes ($P < 0.01$, two-tailed Mann-Whitney U); open symbols denote electrodes that did not meet our significance threshold. This maze complexity effect also appear in the average power spectra for long (blue plots) vs. short (green plots) mazes, shown for selected electrodes (**d**–**g**).

Methods

Subjects. Our three subjects were of average range personality and intelligence and were all able to learn the mazes. Subject 1 (female, age 16) and subject 3 (male, age 19) performed within the range of college students, while subject 2 (male, age 14) had more difficulty. Our research protocol was approved by the institutional review board at Children's Hospital and we obtained informed consent from subjects and their guardians.

Procedure. Subjects learned to navigate computer-rendered multiple-T-junction mazes. Because their visual features were uniform, the mazes offered subjects no information about their position. The subjects' position and viewing angle were manipulated to simulate virtual movement. A subject could move in three different ways: pressing the forward/up arrow key moved the subject down a corridor over the course of 280 ms, and pressing the left or right arrow instantly changed the subject's view by 90 degrees in the respective direction. The maze had to be navigated completely from start to finish. Although these constraints compromised some of the freedom of the subjects to move *ad lib* through a maze, they equated the data format across error-free trials. The sequence of successive turns excluded maze sequences with three consecutive turns in the same direction, preventing the maze from crossing itself. We created a random pool of 6-, 8- and 12-junction mazes. Invisible barriers kept subjects from moving down incorrect corridors.

One testing session involved navigating 20 different mazes. The first four mazes were practice mazes (8-junction), excluded from analysis. Eight mazes were short (6-junction) and eight were long (12-junction), presented in random order. Subjects 2 and 3 each performed one session and subject 1 performed two sessions.

Intracranial EEG recording. Grids and strips contained multiple platinum electrodes with inter-electrode spacing of 1 cm. The locations of the electrodes were determined using co-registered postoperative computed tomograms and preoperative magnetic resonance imaging by an indirect stereotactic technique[25]. The iEEG signal was amplified, band-pass filtered (0.5–100 Hz single pole), digitized at 200 Hz, recorded on analogue videotape using Telefactor apparatus and then copied from videotape to disk. In this conversion process, degradation of the recording medium caused the loss of occasional samples. Missing samples were assigned interpolated values equal to the average of the two adjacent sample values.

Spectral analysis. Spectrograms (Fig. 2b) were computed using a Morlet wavelet transform[27] with a sliding window (16 cycles) in 0.5 Hz increments. spectrogram values were thresholded at mean + one standard deviation ($z = 1$) computed from all maze trials across all wavelet windows. Average power spectra were computed in MATLAB™ with a Welch's window (window, 2 s; overlap, 1 s). Trial power (Fig. 2c) was computed across all fast Fourier-transform windows for the trial. Power spectra for a given maze length (Fig. 3d–g) were computed across all windows in all trials of mazes with a given length. A theta episode is defined as a duration longer than 500 ms (roughly three theta cycles) throughout which the power exceeds $z = 1$ (relative to the distribution of wavelet-window power across all maze trials) on at least one frequency in the range 4–8 Hz (1 Hz increments). For a given trial, the percentage of maze trial time spent in theta episodes (P_θ) is the total time in theta episodes divided by the total time in the trial.

Resections. All subjects underwent subsequent resection of epileptogenic tissue (subject 1, right frontal lobe focus 2 cm × 3 cm, involving orbital gyrus; subject 2, right inferior occipital and inferomedial temporal cortex from a posterior approach; subject 3, standard anterior left temporal lobectomy, including amygdala and some hippocampus).

Received 5 February; accepted 12 April 1999.

1. Winson, J. Loss of hippocampal theta rhythm results in spatial memory deficit in the rat. *Science* **201**, 160–163 (1978).
2. O'Keefe, J. & Recce, M. Phase relationship between hippocampal place units and the EEG theta rhythm. *Hippocampus* **3**, 317–330 (1993).
3. Skaggs, W. E., McNaughton, B. L., Wilson, M. A. & Barnes, C. A. Theta phase precision in hippocampal neuronal populations and the compression of temporal sequences. *Hippocampus* **6**, 149–172 (1996).

4. Bland, B. H. The physiology and pharmacology of hippocampal formation theta rhythms. *Prog. Neurobiol.* **26,** 1–54 (1986).
5. Stewart, M. & Fox, S. E. Hippocampal theta activity in monkeys. *Brain Res.* **538,** 59–63 (1991).
6. Huerta, P. T. & Lisman, J. E. Heightened synaptic plasticity of hippocampal CA1 neurons during a cholinergically induced rhythmic state. *Nature* **364,** 723–725 (1993).
7. Buzsaki, G. Two-stage model of memory trace formation: role for "noisy" brain states. *Neuroscience* **31,** 551–570 (1989).
8. Sohal, V. S. & Hasselmo, M. E. GABA(B) modulation improves sequence disambiguation in computational models of hippocampal region CA3. *Hippocampus* **8,** 171–193 (1998).
9. Buzsaki, G. The hippocampo-neocortical dialogue. *Cereb. Cortex* **6,** 81–92 (1996).
10. Lisman, J. E. & Idiart, M. A. Storage of 7+/−2 short-term memories in oscillatory subcycles. *Science* **267,** 1512–1515 (1995).
11. Buzsaki, G. Memory consolidation during sleep: a neurophysiological perspective. *J. Sleep Res.* **7,** 17–23 (1998).
12. Jensen, O. & Lisman, J. E. An oscillatory short-term memory buffer model can account for data on the Sternberg task. *J. Neurosci.* **18,** 10688–10699 (1998).
13. Borst, J. G., Leung, L. W. & MacFabe, D. F. Electrical activity of the cingulate cortex. II. Cholinergic modulation. *Brain Res.* **407,** 81–93 (1987).
14. Slawinska, U. & Kasicki, S. Theta-like rhythm in depth EEG activity of hypothalamic areas during spontaneous or electrically induced locomotion in the rat. *Brain Res.* **678,** 117–126 (1995).
15. Routtenberg, A. & Taub, F. Hippocampus and superior colliculus: congruent EEG activity demonstrated by a simple measure. *Behav. Biol.* **8,** 801–805 (1973).
16. Halgren, E., Babb, T. L. & Crandall, P. H. Human hippocampal formation EEG desynchronizes during attentiveness and movement. *Electroencephalograph. Clin. Neurophysiol.* **44,** 778–781 (1978).
17. Arnolds, D. E. A. T., Lopes Da Silva, F. H., Aitink, J. W., Kamp, A. & Boeijinga, P. The spectral properties of hippocampal EEG related to behaviour in man. *Electroencephalogr. Clin. Neurophysiol.* **50,** 324–328 (1980).
18. Tesche, C. D. Non-invasive detection of ongoing neuronal population activity in normal human hippocampus. *Brain Res.* **749,** 53–60 (1997).
19. Aguirre, G. K., Detre, J. A., Alsop, D. C. & D'Esposito, M. The parahippocampus subserves topographical learning in man. *Cerebral Cortex* **6,** 823–829 (1996).
20. Maguire, E. A. *et al.* Knowing where and getting there: a human navigation network. *Science* **280,** 921–924 (1998).
21. Epstein, R. & Kanwisher, N. A cortical representation of the local visual environment. *Nature* **392,** 598–601 (1998).
22. Maguire, E. A., Frackowiak, S. J. & Frith, C. D. Learning to find your way: a role for the human hippocampal formation. *Proc. R. Soc. Lond. B* **263,** 1745–1750 (1996).
23. Maguire, E. A., Frackowiak, S. J. & Frith, C. J. Recalling routes around London: activation of the right hippocampus in taxi drivers. *J. Neurosci.* **17,** 7103–7110 (1997).
24. Sperling, M. R. Clinical challenges in invasive monitoring in epilepsy surgery. *Epilepsia* (Suppl.) **38,** S6–S12 (1997).
25. Talairach, J. & Tournoux, P. *Co-planar Stereotaxic Atlas of the Human Brain* (Verlag, Stuttgart, 1988).
26. Tulving, E. *Elements of Episodic Memory* (Oxford Univ. Press, New York, 1983).
27. Grossmann, A. & Morlet, J. *Mathematics + Physics* Vol. 1 (World Scientific, Singapore, 1985).

Acknowledgements. This work was supported by NIH. We thank J. Lisman for encouraging our search for theta; J. Lisman and O. Jensen for helpful discussions during the course of this research; and E. Tulving, E. Marder, L. Abbott and E. Menschik for helpful comments on a previous version of this manuscript. We acknowledge the cooperation of colleagues in the Children's Hospital Epilepsy program including P. M. Black, B. Bourgeois, F. Duffy and L. Kull. Finally, we thank the patients and their families for their participation and support.

Correspondence and requests for materials should be addressed to M.J.K. (e-mail: kahana@brandeis.edu).

The prolyl isomerase Pin1 restores the function of Alzheimer-associated phosphorylated tau protein

Pei-Jung Lu*, Gerburg Wulf*, Xiao Zhen Zhou*, Peter Davies† & Kun Ping Lu*

* *Cancer Biology Program, Division of Hematology/Oncology, Department of Medicine, Beth Israel Deaconess Medical Center and Harvard Medical School, Boston, Massachusetts 02215, USA*
† *Department of Pathology, Albert Einstein College of Medicine, Bronx, New York 10461, USA*

One of the neuropathological hallmarks of Alzheimer's disease is the neurofibrillary tangle, which contains paired helical filaments (PHFs) composed of the microtubule-associated protein tau[1,2]. Tau is hyperphosphorylated in PHFs[3–5], and phosphorylation of tau abolishes its ability to bind microtubules and promote microtubule assembly[6,7]. Restoring the function of phosphorylated tau might prevent or reverse PHF formation in Alzheimer's disease. Phosphorylation on a serine or threonine that precedes proline (pS/T–P) alters the rate of prolyl isomerization and creates a binding site for the WW domain of the prolyl isomerase Pin1 (refs 8–14). Pin1 specifically isomerizes pS/T–P bonds and regulates the function of mitotic phosphoproteins[8–10,12]. Here we show that Pin1 binds to only one pT–P motif in tau and co-purifies with PHFs, resulting in depletion of soluble Pin1 in the brains of Alzheimer's disease patients. Pin1 can restore the ability of phosphorylated tau to bind microtubules and promote microtubule assembly *in vitro*. As depletion of Pin1 induces mitotic arrest and apoptotic cell death[8], sequestration of Pin1 into PHFs may contribute to neuronal death. These findings provide a new insight into the pathogenesis of Alzheimer's disease.

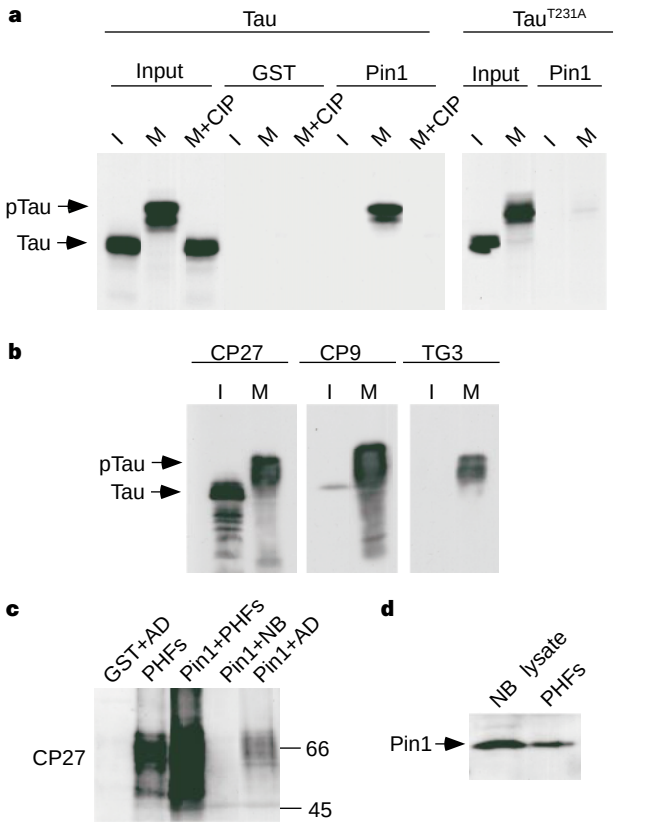

Figure 1 Interaction of Pin1 with pTau and Alzheimer's disease tau, but not with pTau^{T231A}. **a**, *In vitro* translated tau and its mutant were incubated with interphase (I), mitotic extracts (M) or mitotic extracts followed by dephosphorylation with phosphatase (M + CIP), and then separated on SDS–PAGE directly (input) or after purification with GST (GST) or GST–Pin1 (Pin1) beads. **b**, Tau was phosphorylated by I or M extracts and immunoblotted with monoclonal antibodies with different specificity: CP27, all tau forms; CP9, pT231 tau; TG3, an Alzheimer-specific conformation of pT231 tau. **c**, Beads containing GST–Pin1 or GST were incubated with normal brain (NB) or Alzheimer's disease (AD) brain extracts, or PHFs, and bead-associated proteins were immunoblotted with CP27. Lane 1, GST + AD; lane 2, PHFs; lane 3, GST-Pin1 + PHFs; lane 4, GST-Pin1 + NB; lane 5, GST-Pin1 + AD. **d**, PHFs were purified from AD brain extracts and immunoblotted with Pin1 antibodies. Pin1 present in normal brain extracts was used as a control.

Pin1 is a highly conserved and essential mitotic regulator[10,12–15]. It contains an amino-terminal WW domain, a phosphoserine-binding module interacting with specific pS/T–P motifs[13], and a unique carboxy-terminal prolyl isomerase domain that specifically isomerizes pS/T–P bonds[10]. Pin1 binds and regulates the function of a subset of mitotic phosphoproteins, most of which are also recognized by MPM-2, a mitosis- and phosphorylation-specific monoclonal antibody[10,12–15]. As tau is an MPM-2 antigen that is phosphorylated on multiple S/T–P motifs during mitosis[16], we tested whether Pin1 binds tau. Pin1 bound tau only after mitosis-specific phosphorylation, and the binding was abolished by dephosphorylation (Fig. 1a). Thus, Pin1 binds tau in a mitosis-specific and phosphorylation-dependent manner, as shown for other binding proteins[12]. Mitotic events are aberrantly activated in the brains